Nanoscale Advances

ROYAL SOCIETY OF CHEMISTRY

PAPER

View Article Online
View Journal | View Issue

Cite this: *Nanoscale Adv.*, 2022, **4**, 1199

Functionalized polyurethane composite gel electrolyte with cosensitized photoanode for higher solar cell efficiency using a passivation layer†

Ravi Prakash,[a] Ishwar Chandra Maurya,[b] Pankaj Srivastava,[b] Sourov Mondal,[b] Biswajit Ray [b] and Pralay Maiti *[a]

Graphene oxide was chemically tagged with thermoplastic polyurethane, chain extended using butanediol to obtain the varying molecular weight of the polymer. Graphene-tagged polyurethane was functionalized using propane sultone to introduce the polar sulphonate groups in the main chain. The chain extension, tagging of GO and functionalization have been verified through spectroscopic techniques such as NMR, FTIR, UV and gel permeation chromatography. Thermal stability and the nature of the interaction were explored through thermal measurements to understand the effect of GO and functionalization. Electrical conduction was improved by the chemical attachment of graphene with the polymer (5.08×10^{-7} S cm^{-1}), which further increases through functionalization and subsequent use of the additive (1.07×10^{-3} S cm^{-1}) and make them suitable for gel electrolyte, being in the range of semiconductors. Quantum dots of CdS and CdSe were prepared using a capping agent and their characteristic properties and dimensions were worked out for their suitability as active materials in a solar cell. The optical band gap of quantum dots and HOMO/LUMO band structure of functionalized polyurethanes were measured using UV-vis and cyclic voltammetry, and thereby, constructing the overall energy diagrams for a possible combination of materials. Conducting carbon has been incorporated in the gel electrolyte to modulate the conductivity, while the ZnSe layer has been inserted as a passivation layer between the active material and the gel electrolyte. Solar cell devices were fabricated using the suitable materials, through the suitable energy diagram, and found a significantly high power conversion efficiency of 1.71%. The reason behind the improved efficiency is understood from the greater light harvesting behaviour, higher level of conductivity and blocking capacity of the various layered structures to reduce the electron–hole pair recombination.

Received 11th November 2021
Accepted 12th January 2022

DOI: 10.1039/d1na00801c

rsc.li/nanoscale-advances

Introduction

The energy crisis is one of the important issues for human society around the world. Thus, researchers are trying to discover novel renewable clean energy resources to fulfill the energy demands of society.[1,2] The energy demand has enhanced 16 times in the 21st century along with the world population and this energy demand is increasing day by day at a greater efficient rate. The largest renewable power source of our systems is solar irradiation. The total energy received from Sun at the earth's surface is estimated to be 1.2×10^5 TW every year, which is about 6000 times more than the present human power consumption.[3] Photovoltaic devices, which convert solar energy directly into electricity, are the effective and abundant renewable energy devices available through the photo-electric phenomenon, which needs highly efficient power conversion at a lower cost.[4,5] Dye-sensitized solar cells (DSSCs) have attracted researchers over the last two decades because of their high efficiency and relatively inexpensive fabrication process as compared with conventional solar cells.[6,7] Recently, there has been significant interest in solar cells based on perovskite absorbers,[8,9] which enable complete light absorption in considerably thinner films.[7] However, the perovskite solar cells suffer from moisture-sensitive characteristics along with stability issues for fabrication. DSSCs are alternative devices for conventional silicon-based solar cells. It consists of ruthenium-based organic dye molecules as a light harvester, which is attached to a TiO_2 thin film and can achieve up to 11.5% power conversion efficiency. Gratzel and O'Regan[10–12] were first to demonstrate DSSCs, which are typically constructed by

[a]*School of Materials Science and Technology, Indian Institute of Technology (BHU), Varanasi-221005, India. E-mail: pmaiti.mst@itbhu.ac.in*

[b]*Department of Chemistry, Institute of Science, Banaras Hindu University, Varanasi-221005, India*

† Electronic supplementary information (ESI) available. See DOI: 10.1039/d1na00801c

sandwiching the liquid electrolyte in between the counter electrode and working electrode. FTO coated glass was used as substrate and a wide band gap semiconductor like TiO_2 has been deposited on it. Dye molecules were loaded on the FTO/TiO_2 layer, which acted as a sensitizer and Pt was used as a counter electrode. The specific energy of light falling onto dye molecule results in the generation of photo-excited electrons, which are injected into the conduction band of the semiconductor (TiO_2), and redox electrolytes were used to reduce the oxidized form of dye molecules. The oxidized redox electrolytes are reduced in the Pt counter electrode, resulting in a significant amount of electric current flow. Subsequently, the organic dye molecules were replaced by inorganic QDs, considered as sensitizers. Quantum dot solar cells have attracted attention in the modern era because of their low production cost, easy fabrication process and acceptable power conversion efficiency. The inorganic QDs have lot more advantages as compared to dye molecules: (1) high extinction coefficient;[13,14] (2) generation of multiple excitons through single-photon absorption;[15] (3) tuneable band gap;[16] and (4) high photostability corresponding to water and oxygen.[17,18] The maximum theoretical power conversion efficiency of these devices is in order of 44%.[5,19,20] The surface passivation layer usually enhance the performance of QDSSCs,[21] and this layer can form a uniform barrier layer to separate the photoanode with QDs and electrolytes as well as repair the surface defects of the QDs.[16] Well designed passivation can reduce the electron recombination effectively and the layer promotes the separation process of electrons and holes.[22,23] The higher value of the conduction band edge of ZnS as compared to that of CdS/CdSe helps inhibit the transfer of electrons from the conduction band of QDs to LUMO levels of the electrolytes, and hence, usually used as a passivation layer. ZnSe is one of the suitable inorganic passivation materials to form a type of core–shell structure for CdS/CdSe QDs because of its suitable band structure and it has been widely used for QDSSC passivation.[24] Huang *et al.* have demonstrated that type of band alignment would not only prevent electron back transfer to the electrolytes but may also facilitate the desired hole transport from the QDs to electrolytes because both E_{cb} and E_{vb} of ZnSe are higher than those of CdS/CdSe QDs.[25,26] However, ZnSe with a wide band gap and desirable electronic structure does not allow absorption in the long-wavelength regions.[16,24] The electrolytes have an important role in QDSSCs, which can complete the circuit by transferring of the hole to the counter electrode after receiving the holes from the valence band of QDs. The I^-/I_3^- liquid electrolytes show the highest efficiency in DSSC, but these electrolytes cannot be effectively used in QDSSCs because of their corrosive character,[27,28] sealing leakage and easy evaporation.[29] To overcome such issues, polymer electrolytes are the alternative materials of liquid electrolytes in QDSSCs. Polymer electrolytes were used to overcome problems such as corrosion of electrodes, leaking and sealing, shape flexibility, flammability issues and electrochemical stability. Polymer electrolytes are defined as a polymeric material complex with salt.[29,30] Polar functional groups in the main polymeric chain act as a medium to solvate the ionic species through intermolecular interactions and the ionic transport to occur by diffusion of the dissociated ions and their transport through the free volume of polymer matrix.[29,31] Polyurethane (PU) polymer matrix was functionalized to prepare polymer gel electrolytes, which were used to fabricated QDSSCs with co-sensitized CdS/CdSe photoanode to obtain 1.5% power conversion efficiency,[32] and Kumar *et al.*[33] used the functionalized thermoplastic polyurethane gel electrolytes in QDSSCs with TiO_2/CdS photoanode to achieve the PCE of 1.25%. Recently, PU–GO nanocomposites have attracted the attention of many researchers, especially, as the mechanical and electrical properties of nanocomposites were significantly enhanced by adding only 1 wt% of GO during the polymerisation stage.[34,35] To enhance the properties of polymeric materials, composites are prepared by incorporating a small quantity of the filler in the polymer matrix.[36] The polymer composites having low density and good thermal stability,[37] better mechanical properties[38] and higher electrical conductivity of polymer were increased by incorporation of the nanofiller in the polymer matrix.[39] The shifting of the peak position in spectroscopic measurements and lowering of melting temperatures are indicators of the extent of interaction.

In this work, an *in situ* polymerization process was adopted to obtain the chemically tagged graphene oxide polyurethane polymer matrix (PU–GO), which is further functionalized to get a novel polymer gel electrolyte, *i.e.*, the hole transport agent in QDSSCs. The prepared polymer gel electrolytes were used to fabricate QDSSCs with the cosensitized TiO_2/CdS/CdSe photoelectrode. The optimum amount of the ZnSe passivation layer was deposited on the photoanode to reduce the electron–hole pair recombination as well as to increase the light-harvesting efficiency and also to enhance the photovoltaic performance of the fabricated QDSSCs. The underlying reasons are explored in detail.

Experimental

Materials

Cadmium nitrate (Sigma-Aldrich), sodium sulphide (Himedia), TiO_2 paste (Solaronix), graphite flake (Sigma-Aldrich), sodium hydride (NaH), poly(tetramethylene glycol) (PTMG, $M_n = 2900$ g mol^{-1}), butane-di-ol (Sigma-Aldrich), 4,4′-diphenylmethane diisocyanate (MDI, Sigma-Aldrich), titanium tetrachloride ($TiCl_4$, Strem), *N*,*N*-dimethylacetamide (DMA), dibutyl tin dilaurate (DBTDL), propane sultone (Sigma-Aldrich), and ethanol were used for the synthesis process.

Synthesis of CdS QDs

CdS QD were synthesised following a previously reported method.[32,40] 0.4 M cadmium nitrate solution was mixed with 0.114 M ethylenediamine tetraacetic acid (EDTA) solution under constant stirring and heated at 100 °C for 2 h by maintaining the pH ~ 5. Further, 0.11 M sodium sulphide solution was added drop-wise in the reaction mixture and a pale-yellow precipitate was obtained after 30 min. To remove the unwanted species, QDs were washed with water and ethanol

several times and centrifuged at 5000 rpm for 5 min. The prepared QDs were dispersed in chloroform at −5 °C.

Synthesis of CdSe QDs

CdSe QDs were synthesised using the hot injection method with some alteration.[41] The CdSe QDs synthesis was performed in two steps; firstly, a selenium precursor was prepared by dissolving 30 mg of selenium powder in 5 mL octadecene and 0.4 mL tryoctyl phosphine was added drop-wise in solution and was heated at 50 °C for 30 min to obtain the transparent solution. In the second step, 13 mg cadmium oxide was dissolved in 10 mL octadecene and 0.6 mL of oleic acid in an inert atmosphere and the mixture was heated at 223 °C until a transparent solution was obtained. At this temperature, the selenium precursor solution was added to the reaction mixture and 1 mL aliquots were withdrawn at different time intervals using Pasteur pipette to obtain different particle size CdSe QDs. The precipitate was cooled to room temperature and was washed with ethanol and centrifuged at 3000 rpm for 5 min and was redispersed in hexane for further use.

Deposition of ZnSe passivation layer. The ZnSe passivation layer was deposited on the prepared TiO_2/CdS/CdSe photoanode by the SILAR method.[15] TiO_2/CdS/CdSe electrodes were alternately dipped in an aqueous solution of 0.1 M zinc acetate dehydrated for 5 min at 50 °C and were washed with deionized water, dried and subsequently dipped in Na_2SeSO_3 at 50 °C for 5 min and the cycle was repeated thrice.

Synthesis of graphene oxide. Graphene oxide (GO) was synthesised following previously reported modified Hammer's method.[42,43] In this method, 3.0 g graphite flakes (1 equiv.) were dissolved in 400 mL of the mixture of concentrated H_2SO_4 and H_3PO_4 (9 : 1 volume ratio) and 18 g $KMnO_4$ (6 equiv.) was added to the reaction mixture. The reaction mixture was heated at 50 °C with constant stirring for 12 h and the reaction was cooled at room temperature using an ice bath, followed by the addition of 3 mL of 30% H_2O_2 and further washed with dilute HCl, ethanol and distilled water. The reaction mixture was then centrifuged at 5000 rpm for 15 min, and this process was repeated until the medium pH was ∼7. The synthesised GO was dried at 70 °C under vacuum for 48 h.

Synthesis of GO-tagged polyurethane. Polymer synthesis was carried out in three stages of polymerization process[32,33,43] with some alteration. In a typical PU–GO polymer synthesis, the first step involved the formation of prepolymer (PP) by mixing the poly(tetramethylene glycol) (PTMG) and 4,4′-methylene diphenyldiisocyanate in dimethylformamide solvent at 70 °C in the presence of nitrogen atmosphere for 3 h to form an isocyanate-terminated prepolymer. GO (5 mg) was added to the reaction mixture that was heated at 70 °C for 2 h with constant stirring to form GO–prepolymer (PP–GO). Further, butanediol was added as a chain extender along with few drops of DBTDL catalyst (0.1 mL of 1 wt% toluene solution) to complete the polymerization reaction and the reaction mixture was maintained at 70 °C for 24 h with rapid stirring. The PU–GO polymer precipitate was obtained by pouring the solution in deionized water and was dried at 50 °C in vacuum oven for 72 h.

Functionalization of GO–polyurethane. The PU–GO polymer was functionalized *via* a bimolecular nucleophilic substitution reaction. Initially, the pure polymer was dissolved in DMA solvent at 50 °C and the reaction mixture was cooled at −5 °C in a nitrogen atmosphere and NaH was added to the reaction mixture with rapid stirring for 1.5 h. The reaction mixture was brought to room temperature and propane sultone was added and heated at 50 °C for 3 h. The functionalized polymer (SPU–GO) was obtained by pouring the mixture in toluene to precipitate the ionomer and washed with ethanol and dried in a vacuum oven at 72 h.

Preparation of gel electrolytes. The ionomer was dissolved in DMF solvent and was heated at 80 °C with constant stirring to obtain a homogeneous mixture and different weight percentages of conductive carbon were added to the mixture followed by cooling at 5 °C for 18 h to obtain a semisolid ionomer gel (SPU–GO–CC).

Characterisation

Spectroscopic measurements. The absorbance spectroscopy measurements on the synthesised QDs and thin-film polymers were performed using a JASCO V-650 UV-visible spectrophotometer in the spectral range of 200–800 nm at a scan rate of 2 nm s^{-1}. An Alpha Bruker Eco-ATR furnished with a ZnSe ATR crystal was used to obtain the Fourier transform infrared transmittance spectra of QDs and polymers in the spectral range 600–4000 cm^{-1} by taking 100 scans with 4 cm^{-1} resolution. Proton (^1H) NMR spectroscopic measurements (Bruker Biospin, 500 MHz) were performed for the functionalized polymers and the chemical shifts were recorded in ppm (δ). DMSO-d_6 was used as a solvent. All spectroscopic measurements were performed at room temperature.

Thermal analysis. The thermal stability of pure and functionalised PUs was estimated using a Mettler-Toledo thermogravimetric analyzer (TGA) in the temperature range of 40 to 600 °C at a heating rate of 20 °C min^{-1}. Differential scanning calorimetry (DSC) (Mettler 832) was used to estimate the melting temperature and heat of fusion of pure and various degrees of functionalized PUs. The temperature range was from −40 to 200 °C with heating and cooling rates of 10 °C min^{-1} and 5 °C min^{-1}, respectively, under the flow of nitrogen.

Electrochemical measurement

Electrochemical impedance spectroscopy. The conductivity of pure and functionalized polymer was determined using the four-probe AC impedance experiments using multichannel Autolab M204 (potentiostat/galvanostat) with FRA 32 (Frequency Response Analyzer) in the range of 0.1 to 10^6 Hz. The polymer was clipped between two circular titanium electrodes with a surface area of 3.14 cm^2. The operational applied frequency range was from 0.1 to 10^6 Hz at the scan rate of 1 μA s^{-1}. Before measuring the sample, a blank spectrum (Nyquist plot) was recorded to take care of the wire resistance. The resistance of the polymer was calculated from the fit and simulation methods using the Nova software (2.1.4 version) and

the resistance of the polymer was used to calculate the ionic conductivity using the following eqn (1)

$$\kappa^{m}(\mathrm{S\ cm^{-1}}) = \frac{L(\mathrm{cm})}{[R(\Omega) \times A(\mathrm{cm^2})]} \quad (1)$$

where, κ^{m} is the ionic conductivity of the polymer, R is the resistance of polymer, A is the area of polymer, L is the distance between two electrodes. The activation energy was calculated using the following equation

$$\sigma = \sigma_0 \exp - \frac{E_a}{RT} \quad (2)$$

where E_a is the activation energy, R is constant, T is temperature, σ is the ionic conductivity.

Cyclic voltammetry. A Metrohm Autolab M204 potentiostat/galvanostat with a three-electrode system Ag/AgCl as a reference electrode, glassy carbon as the working electrode and platinum as a counter electrode was used to perform cyclic voltammetry (CV) measurements on polymer and QDs. The CV measurement was used to calculate the HOMO (highest occupied molecular orbital) and LUMO (lowest unoccupied molecular orbital) levels of polymers and QDs. The HOMO and LUMO of the energy level of the polymer and QDs were calculated taking ferrocene as reference materials (−4.4 eV).[44]

$$E_{HOMO} = -eV(E_{OX}^{onset} + 4.4) \quad (3)$$

$$E_{LUMO} = -eV(E_{red}^{onset} + 4.4) \quad (4)$$

The finely dispersed sample was prepared by dissolving 2 mg of QDs in 5 mL of *N*-methyl pyrrolidone solvent and ultrasonicated for 15 min for obtaining a fine dispersion of particles. For finding the suitable working potential range, the CV measurement was performed in a blank run with NMP as a solvent. The CV measurements of the prepared samples were carried out at a scan rate of 20 mV s^{-1} with the potential range of −2.5 to +2.5 V at room temperature.

Fabrication of solar cells

Preparation of the photoanode. Firstly, the FTO glass sheet (2 × 1.5 cm^2) was cleaned using a bath sonication process in soap water, acetone and distilled water for 10 min in every case. Thin-film deposition (0.20 cm^2 area) of the TiO_2 paste (Solaronix) on the FTO glass was performed by the doctor blade technique, followed by heating at 75 °C for 30 min to remove the low boiling point organic solvent. It was annealed at 450 °C for 30 min, resulting in a transparent thin film of TiO_2 on FTO glass. The QD deposition was performed following our previously reported method. Briefly, the as-prepared CdS QDs were dispersed in isopropanol by ultrasonication for 15 min and CdS QDs were deposited on the TiO_2 film using a spin coater (Spin NXG-P1) at 1500 rpm for 15 min to form a uniform TiO_2/CdS film. Similarly, CdSe QDs were dispersed in hexane and were deposited on the TiO_2/CdS film, similarly. During the preparation of photoanode, the deposition of each layer of QDs was dried at 75 °C for 30 min to remove the solvent for better film formation. The prepared photoanode was kept in a vacuum under dark conditions at room temperature. It was used in the fabrication of QDSSC devices.

Preparation of counter electrode. The Pt thin film was used as a counter electrode; the doctor blade method was used to deposit the thin film of Pt on FTO glass under the same active area of 0.20 cm^2, followed by heating at 80 °C for 30 min to remove the low boiling organic binder. Subsequently, it was annealed at 450 °C for 30 min and was cooled at room temperature to obtain the uniform Pt thin film. For fabricating QDSSCs, sufficient number of gel electrolytes were spread on the active area of the photoanode and both the electrodes were sandwiched with each other. The 0.25 mm thick thermoplastic non-conducting spacer (Solaronix Meltonix 1170-25) was used between these two electrodes for better contact and prohibited the penetration of gel electrolyte.

Solar cell measurement. A multichannel Autolab M204 potentiostat galvanostat combined with the LED Driver (700 mA output) connected to an optical bench was used to determine the current–voltage (*I–V*) characteristic measurement. The highly focused light source was used using the Autolab LED Driver and the LED light source output was controlled using the programmable software, which was connected to the optical bench. QDSSC performances were characterized in terms of three parameters, short circuit current density (J_{sc}), open-circuit voltage (V_{oc}) and the fill factor (FF) as these are directly responsible for the power conversion efficiency (η) of QDSSCs. These parameters were calculated using the following equations

$$FF = \frac{J_{max}}{J_{sc}} \times \frac{V_{max}}{V_{oc}} \text{ or } FF = \frac{P_{max}}{J_{sc} \times V_{oc}} \quad (5)$$

$$\eta(\%) = \frac{P_{max}}{P_{in}} \times 100 \text{ or } \eta(\%) = \frac{J_{sc} \times V_{oc} \times FF}{P_{in}} \times 100 \quad (6)$$

Results and discussion

Evidence of chemical tagging of GO with polyurethane and functionalization

The schematic reaction of the formation of GO-tagged polyurethane (PU–GO) in three stages of polymerization and subsequent functionalization of polyurethane polymer (SPU–GO) are shown in Scheme 1. ^{1}H NMR and FTIR spectroscopic measurements were used to confirm the chemical tagging of graphene oxide in polymer chains and its subsequent functionalization of the polymer (PU–GO). Fig. 1a shows the ^{1}H NMR patterns of synthesized pure polyurethane (PU), GO-tagged polyurethane (PU–GO) and functionalized GO-tagged polyurethane (SPU–GO). Pure PU showed the peak at a chemical shift of δ = 8.54 ppm for >NH proton[45] while PU–GO showed two peaks for >N–H proton at 8.54 ppm (high intensity) and 8.45 ppm (low intensity) due to the presence of two types of >NH protons in the polymer chain with different chemical environments and the appearance of a new shielded peak at 8.45 ppm (absent in pure PU) is due to the interaction between graphene sheets (electrons rich) and >NH proton[46] in PU–GO polymer, confirming the chemical tagging of GO with the polymer (PU)

chains. The functionalized polymer (SPU–GO) shows a new strong peak at a chemical shift of $\delta = 8.48$ ppm for $-SO_3H$ proton[33] and another two new peaks at $\delta = 1.9$ and 1.6 ppm for $-CH_2$ protons[47,48] of the propane sultone group. This is to mention that these peaks are absent in pure PU and PU–GO polymer, which in turn, confirm the insertion of the sulfonate group in PU–GO polymer chains. In FTIR measurements, the prepolymer (PP) showed a characteristic peak at 3308 cm^{-1} due to the hydrogen-bonded >NH group[49] (stretching vibration) present in the prepolymer chain and the peak at 1778 cm^{-1} is responsible for the imide-carbonyl group[50] present in PP (Fig. 1b).

After grafting of GO in prepolymer chains, the >NH peak is slightly shifted in GO-tagged prepolymer (PP–GO) due to the interaction between the graphene sheet and >NH bonds[46] and the GO-tagged polyurethane-extended polymer (PU–GO) shows a peak at 3305 cm^{-1} for the hydrogen-bonded –NH group[49] present in the hard segment of polyurethane chains. The peak at 1778 cm^{-1} disappears[50] in PU–GO, suggesting the chain extension after the reaction with butanediol.

Further, the hydrogen-bonded >NH peak becomes broad at 3413 cm^{-1} with the sulfonation of the PU–GO polymer[32] and SPU–GO exhibits a new strong peak at 1184 cm^{-1} due to the symmetrical stretching vibration of the S=O linkages after functionalization.

The UV-vis absorption spectroscopic measurement was performed to understand the interactive nature between graphene sheets and polymer chains. Fig. 1c shows the UV-vis absorption patterns of PP, PP–GO, PU–GO and SPU–GO. The prominent peak in PP at 279 nm is due to n → π* transition[51] and it is red shifted to 293 nm in PP–GO due to the presence of the graphene sheet in the prepolymer chain.[43] The peak position has further shifted to 298 nm in PU–GO after chain extension using butanediol. The SPU–GO polymer shows two broad peaks at 305 nm due to n → π* transition of urethane linkage and another one is at 372 nm assigned as n → π* transition due to the presence of the polar sulfonate group in polymer chains.[32,33] However, spectroscopic techniques clearly indicate the tagging of GO with the polyurethane chain and their subsequent sulphonation to convert into SPU–GO as ion conductive species. The molar masses of PP, PP–GO and PU–GO were determined by the gel permeation chromatography (GPC) measurements and are shown in Fig. 1d. Molar masses ($\bar{M}_n$) of PP, PP–GO and PU–GO are 5.2, 5.3 and 6.4 K, respectively, and the molar mass of PU–GO is higher than that of PP–GO after the addition of butanediol as the chain extender in the third stage of the polymerization reaction, which confirms the chain extension of the polymer. The molecular weight decreases after the functionalization of GO-tagged polyurethane and the molecular weight was found to 1.7 K as measured using GPC, presumably due to hydrolysis in the presence of acidic environment.

Thermal stabilities of the prepolymer, polymer and functionalized polymers were estimated using thermogravimetric analysis as shown in Fig. 1e. Both the pure and functionalized polymers show two stages of degradation due to the hard and soft segments of the polymer chain and the functionalized polymer exhibits lower degradation as compared to pure polymer. The weight loss at a lower temperature is due to the degradation of the hard segment of the polymer chain and the soft segment is degraded at high temperature. The initial weight

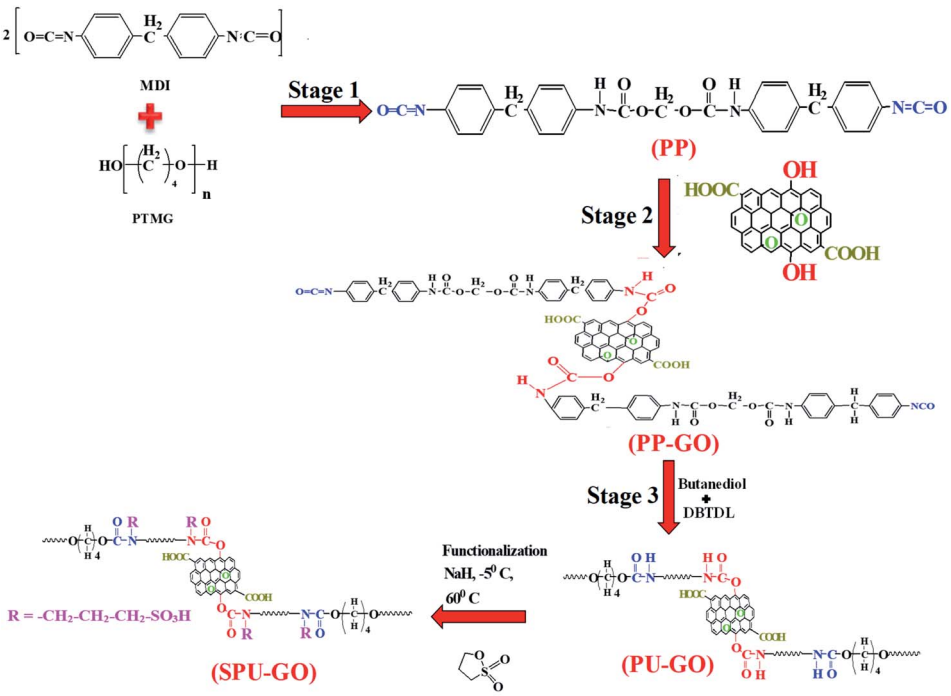

Scheme 1 A reaction scheme for the synthesis of GO-tagged polyurethane (PU–GO) in three stages and its subsequent functionalization (SPU–GO). The designation of polymer is mentioned below with the respective chemical formula.

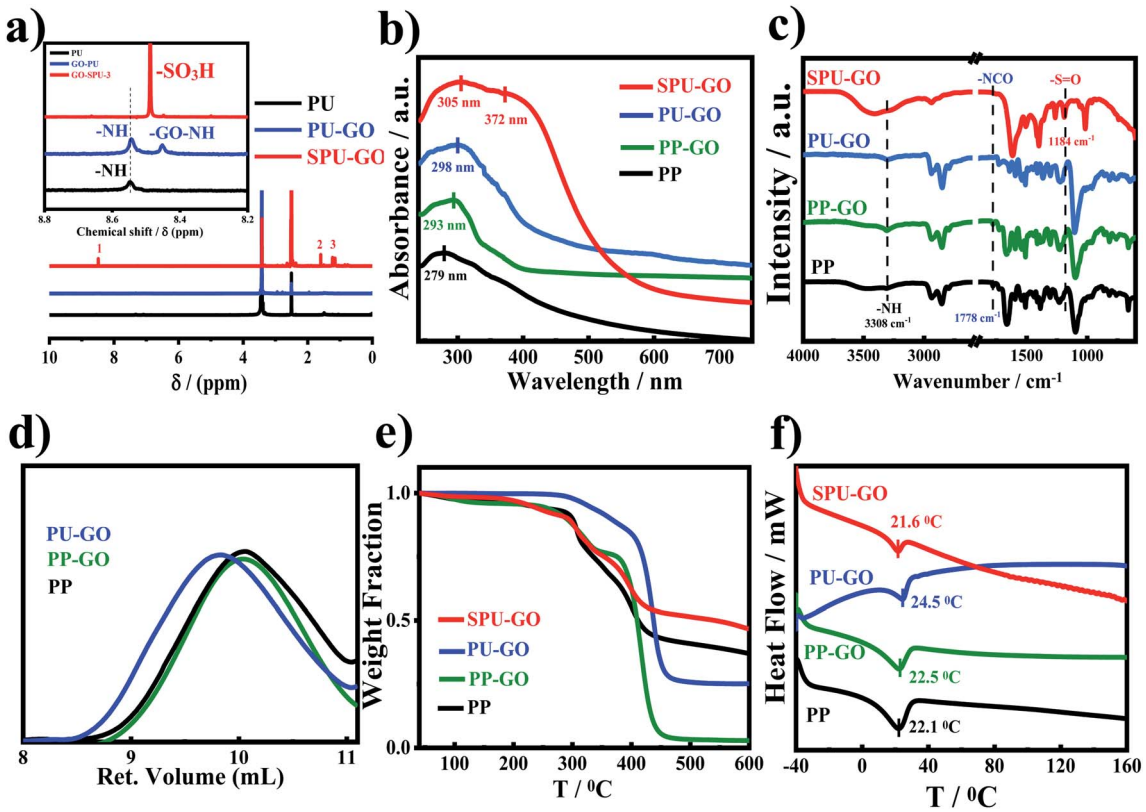

Fig. 1 (a) ^{1}H NMR spectra of pure PU, PU–GO and functionalized polymer (SPU–GO), the inset shows the magnified spectrum in the indicated zone; (b) FTIR spectra of PP, PP–GO, PU–GO and SPU–GO showing the appearance of new peak and shifting of peak position; (c) UV-vis absorption spectra of PP, PP–GO, PU–GO and functionalized polymer (SPU–GO) showing shifting of peak position; (d) gel permeation chromatograms of PP, PP–GO and PU–GO showing relative elution time; (e) TGA thermograms of PP, PP–GO, PU–GO and SPU–GO demonstrating relative thermal stability; and (f) DSC thermograms of PP, PP–GO, PU–GO and SPU–GO showing the melting temperatures.

loss in SPU–GO is observed due to the hydrophilic nature of SPU–GO. The degradation temperatures were found to be 226°, 241°, 327° and 228 °C for PP, PP–GO, PU–GO and SPU–GO, respectively. The presence of graphene enhances thermal stability while sulphonation decreases the thermal stability a bit. This is to mention that the temperature corresponding to 5% weight loss is considered as the degradation temperature. However, the functionalized polymer was thermally stable up to 200 °C and thereby suitable for its application in solar cells. Differential scanning calorimetric measurements were used to analyse the melting behaviour of specimens, as shown in Fig. 1f. The melting temperature of PP was 22.1 °C and the presence of graphene oxide in the prepolymer enhances the crystalline nature of PP–GO, resulting in an increase in its melting temperature to 22.5 °C. The chain extension with butanediol in PP–GO further increases the melting temperature to 24.5 °C. The functionalization of the polymer in SPU–GO showed a melting temperature of 21.6 °C. The melting temperatures corresponding to the soft segment zone and crystallization of the soft segment were facilitated in the presence of graphene, acting as heterogeneous nucleation sites. The heat of fusion values were calculated as 25, 26.5, 27.9 and 6.3 J g^{-1} for PP, PP–GO, PU–GO and SPU–GO, respectively. The functionalization in SPU–GO reduces the crystallinity, both in terms of melting temperature and heat of fusion, predominantly due to the presence of sulphonate groups, which inhibits the main chain to fit into the crystalline lattice. Further, intermolecular interaction enhances in the presence of the sulphonate group in SPU–GO, which causes lowering of melting and heat of fusion as compared to PU–GO. However, the small increase in heat of fusion along with the temperature is noticed in the presence of graphene in PP–GO and PU–GO suggesting enhanced heterogeneous nucleation.

Ionic transport behaviour

The lower resistance of electrolytes is responsible for the better performance of solar cell devices. The prepared gel polymer electrolytes having low resistance with good ionic conductivity may facilitate better transportation of the holes in the operational mode of the devices. Electrochemical impedance spectrometry (EIS) measurements were used to calculate the ionic conductivity of the polymers. The Nyquist plots were used to measure the polarizing resistance of the polymers using the fit and simulation method (Fig. 2a). The resistance of PP was found to be 6.81 × 10^{8} Ω and the introduction of the graphene sheet in the polymer chain reduces the resistance of PP–GO to

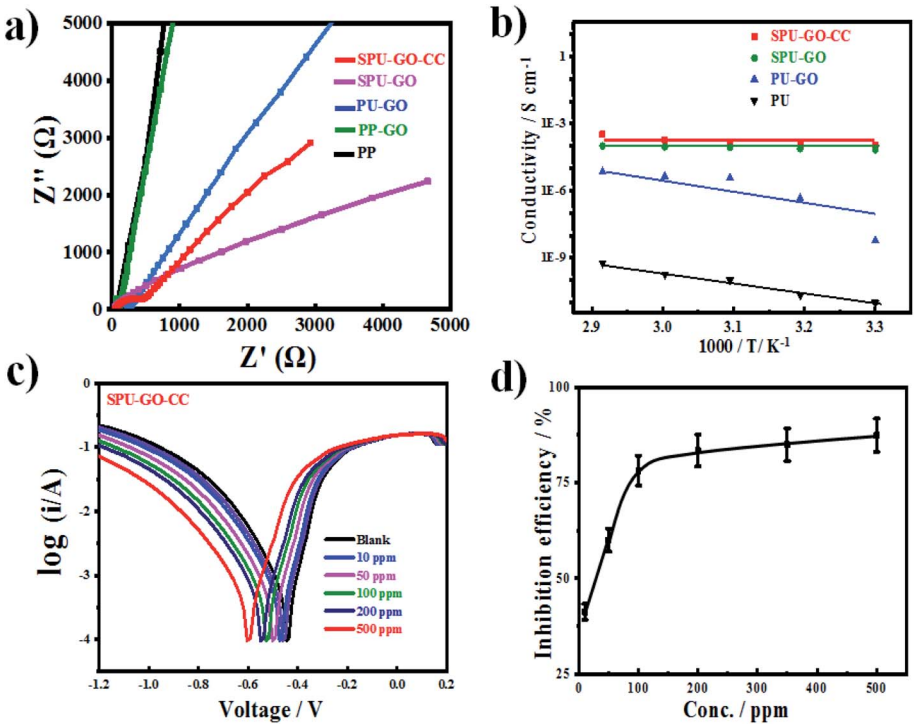

Fig. 2 (a) Nyquist plots for the indicated pure and functionalized PUs; (b) Arrhenius plots of the pure and indicated functionalized polymers; (c) potentiodynamic polarization measurement of mild steel with and without the indicated inhibitors in 0.5 M H_2SO_4 solution; and (d) percentage inhibition efficiency as a function of inhibitor (SPU–GO–CC) concentration.

Table 1 The resistance and conductivities of various pure and functionalized polymer/composite

S. no.	Sample	Resistance (Ω)	Conductivity (S cm^{-1})
1.	PP	6.81×10^8	2.10×10^{-11}
2.	PP–GO	5.28×10^6	1.02×10^{-9}
3.	PU–GO	7.25×10^5	5.08×10^{-7}
4.	SPU–GO	6.25×10^2	2.98×10^{-4}
5.	SPU–GO–CC	5.28×10^2	1.07×10^{-3}

5.67×10^6 Ω due to the presence of graphene sheets, which helped in better transportation of the charge. The resistance was further decreased to 7.25×10^5 Ω in the extended polymer (PU–GO). The attachment of the sulfonate group (ionic moiety) in the main chain in SPU–GO exhibited the resistance of 6.25×10^2 Ω, and the incorporation of 0.052 wt% of the conductive carbon (CC) to the prepared composite (SPU–GO–CC) caused a further decrease in the resistance to 5.28×10^2 Ω. The corresponding conductivities are presented in Table 1. However, the functionalized polymer (SPU–GO) and its composite (SPU–GO–CC) exhibited ionic conductivities in the range of semiconductors (2.98×10^{-4} and 1.07×10^{-3} S cm^{-1}, respectively), hence, they were found suitable for solar cell device fabrication.

The specimens were sandwiched between two titanium electrodes and EIS data were recorded at different temperatures and Arrhenius behaviour of polyurethane, PU–GO, SPU–GO and SPU–GO–CC were plotted/fitted using eqn (2) as shown in Fig. 2b. The activation energies were calculated from the respective slopes of Arrhenius plots. The calculated values of activation energy from the Arrhenius plots were found to be 113.3, 61.5, 9.5 and 9.2 kJ mol^{-1} for pure PU, PU–GO, SPU–GO and SPU–GO–CC, respectively. The reduction of activation energy is due to the presence of the sulphonate group in the main chain and a similar reduction process is reported in the literature using sulfonated PU (~15 kJ mol^{-1}).[52] The lower activation energy for the functionalized polymer is helpful for greater conduction and is likely to be suitable as a gel electrolyte in solar cell applications. From the EIS measurement, it is clearly observed that the ionic conductivities increase by tagging GO, which is further enhanced through functionalization, followed by the addition of conducting carbon.

Corrosion inhibition efficiency

Cell durability plays an important role in fabricating the solar cell device, which depends on the developed materials used in the solar cell. The corrosive nature of the most active ingredients is responsible for the low life cycle of the device. The corrosive nature/property was estimated using the potentiodynamic polarization measurement technique with a three-electrode setup assembled in a glass cell. Mild steel was used as a working electrode, Ag/AgCl as a reference electrode and platinum as a counter electrode. The dimensions of the working electrode were $3 \times 1 \times 0.1$ cm^3 with an active area of 1 cm^2 and was dipped in 0.5 M H_2SO_4 acid solution. The corrosion potential (E_{corr}) and corrosion current densities (I_{corr}) were calculated by extrapolating cathodic and anodic current–

Table 2 Corrosion current density, potential, corrosion rate density and percentage inhibition efficiency of functionalized polymer composites at different concentration

Inhibitor	Inhibitor concentration (ppm)	Corrosion potential (V)	Corrosion rate density (μA cm^{-2})	Inhibition efficiency (%)
Blank	—	0.445	6.445	—
SPU–GO–CC	10	0.459	4.184	35.08
SPU–GO–CC	50	0.472	2.544	60.52
SPU–GO–CC	100	0.500	1.414	78.06
SPU–GO–CC	200	0.528	1.045	83.78
SPU–GO–CC	350	0.548	1.031	84.03
SPU–GO–CC	500	0.602	0.812	87.40

potential characteristics of the linear polarization Tafel plots up to their intersection point. The inhibitor efficiency was calculated from the measured I_{corr} values using the following equation;

$$IE\% = \frac{I^0_{corr} - I_{corr}}{I^0_{corr}} \quad (7)$$

where, I_{corr} and I^0_{corr} are current densities with and without the presence of inhibitors, respectively. The potentiodynamic polarization linear Tafel (*I*–*V*) plots are shown in Fig. 2c. The I^0_{corr} and E^0_{corr} values were observed for the blank coupon (without inhibitor) and were found to be 6.445×10^{-6} A cm^{-2} and −0.445 volt, respectively. The addition of 10 ppm concentration of SPU–GO–CC in the acidic solution decreases the corrosion current densities from 6.445×10^{-6} to 4.184×10^{-6} A cm^{-2} and the corrosion potential was shifted from −0.445 to −0.459 V with inhibitor efficiency (η) of 35%. Table 2 represents the variations of I_{corr}, E_{corr} and inhibitor efficiency (η) upon increasing the inhibitor concentration and the considerably high (87.40%) inhibitor efficiency (η) was observed using 500 ppm concentration of SPU–GO–CC inhibitor (Fig. 2d). However, the developed system (SPU–GO–CC) exhibits anti-corrosive properties with high inhibition efficiency. This is to mention that corrosion inhibition efficiency of 85 to 92% is reported in the literature[43,47] using sulphonated polyurethane, similar results were obtained in this study.

Morphology and optical properties of QDs

The UV-vis absorption spectroscopic measurements on the synthesized CdS and CdSe QDs are shown in Fig. 3a. The characteristic absorption peaks were observed in the visible region for both CdS and CdSe QDs at 492 and 541 nm, respectively.[32,33] The capping of CdS with EDTA plays a significant role

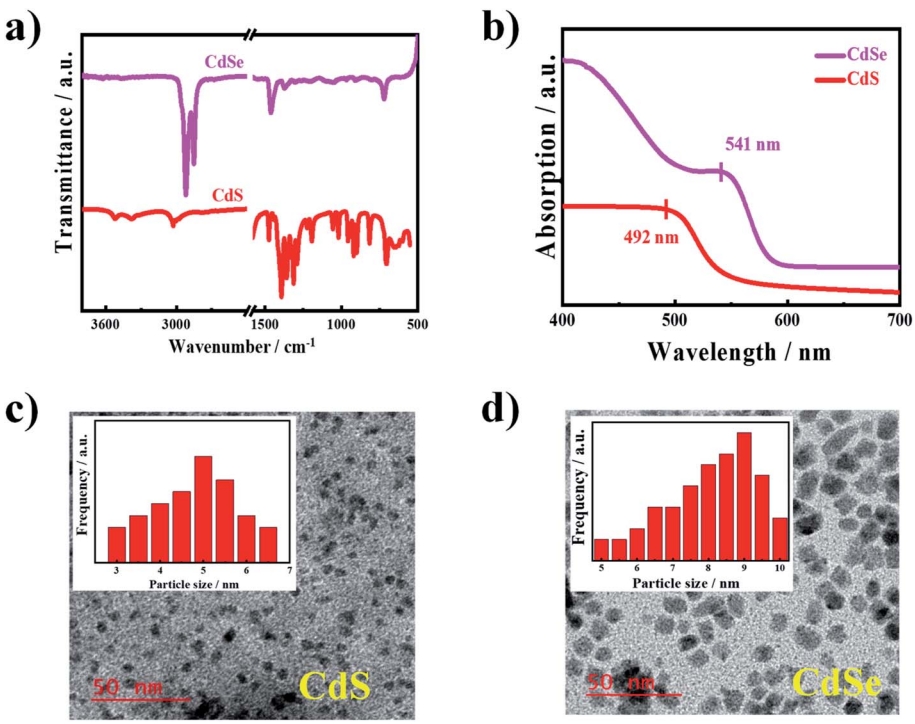

Fig. 3 (a) UV-vis absorption spectra of CdS and CdSe showing the absorption peak; (b) FTIR spectra of the synthesised CdS and CdSe QDs; (c) TEM bright-field image and particle distribution of CdS QDs; and (d) TEM bright-field image and particle size distribution of CdSe QDs.

in the absorption behaviour and the absorption band appears at 532 nm when prepared without any capping agent (ESI Fig. S1†).[53,54] FTIR spectra of the prepared QDs are shown in Fig. 3b. The peak at 3520 cm^{-1} appears for O–H stretching frequency of water molecules, which are absorbed on the CdS surface through hydrogen bonding[55] and the peaks at 705 cm^{-1} in CdS QD are due to the CH– stretching and bending mode of EDTA.[32,47] The CdSe QD shows intense peaks at 2919 and 2850 cm^{-1} due to antisymmetric and symmetric C–H stretching vibrations of the CH_2– group,[56] respectively, due to the capping agent of oleic acid. Other peaks at 1460 and 1373 cm^{-1} are due to antisymmetric and symmetric vibration of the carboxylate anion[57] (COO^-), which confirms that the carboxylic group on the surface of CdSe QDs appears from the capping agent. This is to mention that the peak at 3483 cm^{-1} appears in CdS without any capping agent.[33] The capping agent plays an important role in the size of the quantum dots and the average particle size of the synthesized QDs was determined using transmission electron microscopy (TEM) bright-field images and the average particle sizes were found to be 5 and 9 nm for CdS and CdSe QDs, respectively (Fig. 3c and d). This is to mention that a bigger particle dimension of 15 nm was measured for the quantum dots prepared without any capping agent.[33] CdS and CdSe both are promising materials reported to have better performance in QDSSCs. CdS QDs have a higher band edge than that of TiO_2, which is more beneficial for the excited electron injection from CdS QDs, but the absorption range of CdS QDs are below the wavelength of 550 nm, whereas the absorption range of CdSe QDs may be extended to the 720 nm wavelength and the electron injection efficiency is less than that of CdS QDs, hence, to take both advantages of materials such as electron injection ability and light-harvesting capability of CdS, CdSe QDs were used to prepare the cosensitizer on TiO_2 film. So, the cosensitized photoanode is more effective than the single loaded either CdS or CdSe QDs.

Energy levels through electrochemistry

The cyclic voltammetric (CV) measurements are used to analyse the electrochemical response for electrode–electrolyte interfaces and to calculate the produced current after applying the voltage with a specific scan rate. In the redox reaction, the reduction of polymer chains becomes negatively charged while it is converted into positively charge species during oxidation. CV measurements indicate two peaks; one with a negative current with respect to the reduction process, while the other is for a positive current corresponding to the oxidation process. The onset of oxidation and reduction potential of the CV measurement is used to determine the HOMO and LUMO energy levels of the materials, respectively. The electron and hole transport rates effectively depend upon the HOMO and LUMO energy levels of the materials. The CV measurements used to calculate the HOMO and LUMO energy levels of the pure and various functionalized polymer materials are shown in the ESI Fig. S2† and present the energy profile diagrams for all QDs and polymers to verify the best suitable match for better electron–hole pair transportation during photoexcitation in the constructed devices. Fig. 4a shows the current–potential curves of pure and functionalized polymers. The E_{OX} values for SPU–GO and SPU–GO–CC are 0.76 and 0.64 V, respectively. The E_{HOMO} for SPU–GO and SPU–GO–CC are found to be −5.16 and

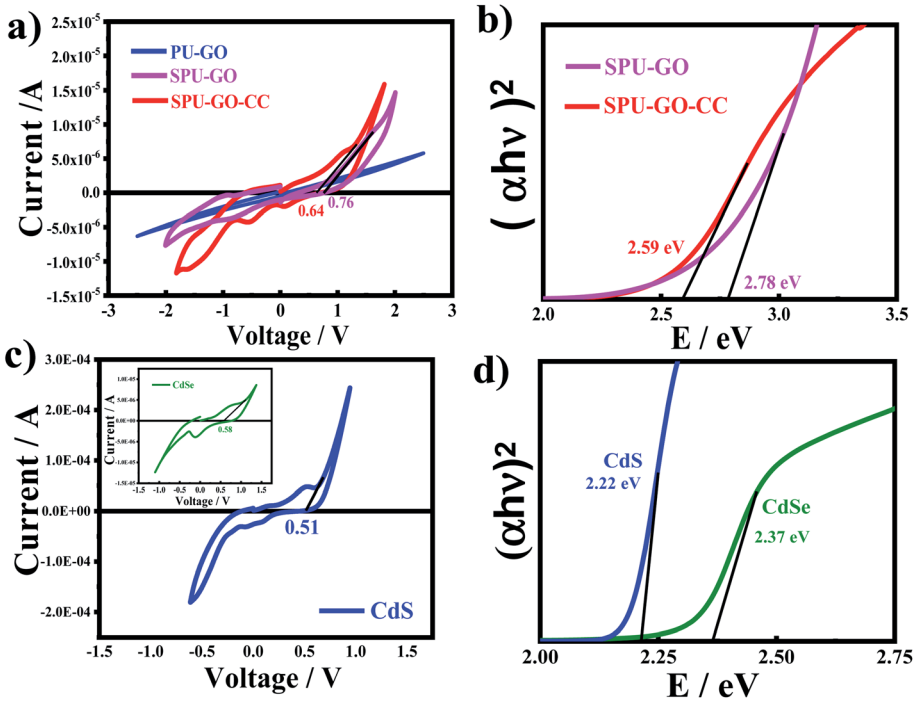

Fig. 4 (a) CV voltammograms of PU–GO, SPU–GO and SPU–GO–CC polymer/composite; (b) optical band gap measurement of SPU–GO and SPU–GO–CC polymer/composite; (c) CV voltammograms of CdS and CdSe QDs; and (d) optical band gap measurements of CdS and CdSe QDs.

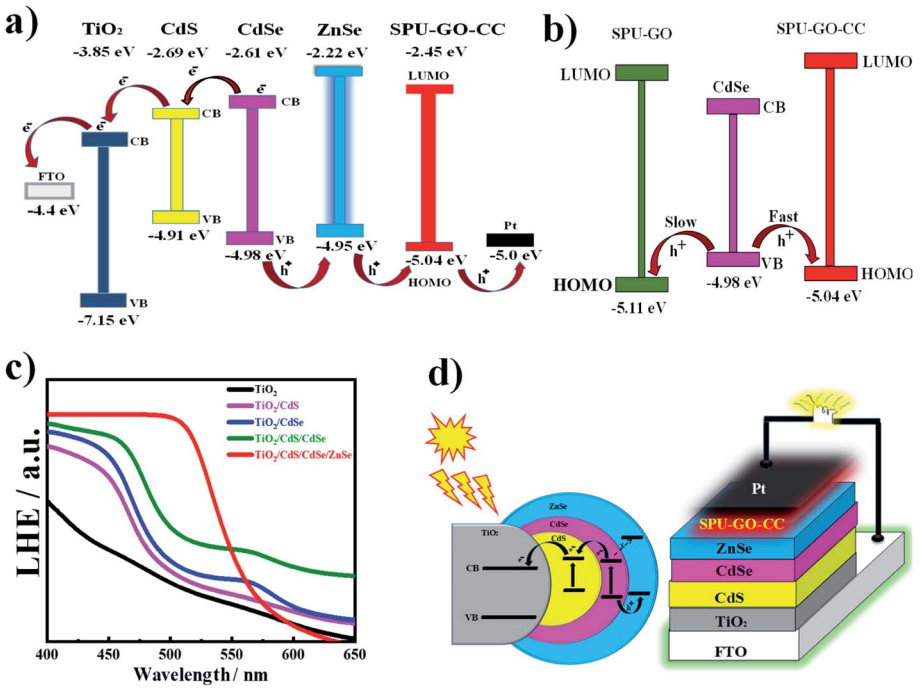

Fig. 5 (a) Energy profile diagram of TiO_2, CdS and CdSe with SPU–GO–CC gel electrolyte; (b) comparison of the energy level of the SPU–GO and SPU–GO–CC with CdSe QDs showing the transport behaviour of holes; (c) light-harvesting efficiency of layer by layer deposition of QDs photoanodes FTO/TiO_2, FTO/TiO_2/CdS, FTO/TiO_2/CdS/CdSe and ZnSe passivation layer; and (d) solar excitation mechanism and layered structure of fabricated QDSSCs.

−5.04 eV, respectively, as calculated using eqn (3), and the optical band gap of SPU–GO and SPU–GO–CC are found to be 2.78 and 2.59 eV, respectively, using the Tauc's plots (Fig. 4b). This is to mention that PU–GO does not exhibit any oxidation and reduction potential in the range studied here, as evident from the linear behaviour of the current–voltage curve. The CV voltammograms of CdS and CdSe QDs are shown in Fig. 4c. The E_{OX} value of CdS is calculated as 0.51 V and the E_{HOMO} and E_{LUMO} values are −4.91 and −2.69 eV, respectively, as calculated using the eqn (3) and (4). Similarly, CV measurement of CdSe QDs are shown in Fig. 4c (inset), and the E_{OX} value is found to be 0.58 V and E_{HOMO} and E_{LUMO} values are −4.98 and −2.61 eV, respectively (Fig. 4d). The electrochemical properties of photoanode are changed with the layered patterns. The open-circuit voltage for TiO_2/CdS, TiO_2/CdSe, TiO_2/CdSe/CdS, TiO_2/CdS/CdSe, and TiO_2/CdS/CdSe/ZnSe photoanodes had the values of 0.36, 0.21, 0.24, 0.54 and 0.73 volts, respectively, as observed through the EIS measurement; hence, the most suitable photoanode was found to be TiO_2/CdS/CdSe/ZnSe with the highest open-circuit voltage of 0.73 V and is used to fabricate the QDSSCs mentioned in the manuscript. The HOMO and LUMO energy levels of all polymers and QDs are combined to draw the energy profile diagrams, which are shown in the ESI Fig. S3,† to understand the suitable match of energy levels for better materials to fabricate solar cells devices. The optimized perfect match of the energy profile diagram of the functionalized polymer with CdS/CdSe QDs along with the respective electrodes is shown in Fig. 5a. The hole transportation is faster from the conduction band of CdSe QDs to E_{HOMO} of SPU–GO–CC, as compared to the SPU–GO due to low energy gap/close proximity between VB of CdSe and E_{HOMO} of SPU–GO–CC as shown in Fig. 5b. Hence, the functionalized composite SPU–GO–CC is a suitable material as a polymer gel electrolyte for the fabrication of solar cells.

Light-harvesting efficiency and passivation layer

It is essential to develop a greater light-harvesting material that eventually generates more excitons under the irradiation of sunlight. The light-harvesting efficiency (LHE) of TiO_2, TiO_2/CdS, TiO_2/CdSe, and TiO_2/CdS/CdSe/ZnSe (ZnSe as the additional layer over the active materials/layer, acting as the passivation layer) is shown in Fig. 5c. Light-harvesting of the combined layers of CdS and CdSe exhibits a red shift in terms of light absorption compared to an individual later of either CdS or CdSe. Light-harvesting of TiO_2/CdS/CdSe/ZnSe is significantly higher compared to that without the passivation layer. Hence, the ZnSe passivation layer has enhanced the LHE, which can help in generating multiple excitons from the overall system. Another important role of the passivation layer is shown in the energy profile diagram, E_{HOMO}, E_{LUMO}, and optical band gap values of ZnSe are −4.95, −2.22 and 2.73 eV, respectively. Two SILAR cycles are used to deposit the passivation layer on QDs surface for the better performance of devices and can be attributed to higher intensity and greater red shift of light absorption in the 400–700 nm range and increases the electron concentration[15] in the TiO_2 substrate, overall sensitized by the CdS/CdSe/ZnSe layer. The energy profile diagram gives more

information about the flow of excited electrons, as shown in Fig. 5a. The photoexcitation mechanism and the layered structure of the fabricated QDSSCs are shown in Fig. 5d. After the absorption of a photon by CdSe QDs, the electron–hole pairs are generated and the electrons are easily transported from the valence band (VB) of CdSe to the CB of CdS through the CB of CdSe and the passivation layer of ZnSe facilitates the hole transportation from the VB of CdSe QDs to the HOMO level of SPU–GO–CC and prohibits the recombination of electron–hole pair, resulting in improved performance of QDSSC devices. Further, the ZnSe passivation layer prohibits the electron transport from the CB band of CdSe to the LUMO level of SPU–GO–CC. The incorporation of the passivation layer between the hole transport layer material and TiO_2/CdS/CdSe cosensitized photoanode prohibits the electron–hole recombination because of the considerable energy-level difference between VB of CdSe QDs and ZnSe (0.39), which is higher, as compared to the LUMO level of the prepared composite polymer gel electrolytes and VB of CdSe (0.16). Hence, back electron transfer is difficult resulting in fewer electron–hole recombinations, as compared to the system without any passivation layer. The introduction of ZnSe as the passivation layer also exhibited a considerable increment of absorbance and red shift in the literature.[58] However, the passivation layer facilitates hole transport while it prohibits electron transport to the gel electrolyte and ultimately suppresses the electron–hole pair recombination phenomena (usually responsible for low energy conversion efficiency).

Photovoltaic performance of QDSSCs

TiO_2/CdS/CdSe cosensitized photoanode is designed along with a polymer gel electrolyte with ZnSe passivation layer have been fabricated in the form of QDSSCs following the scheme presented in Fig. 5d. The photocurrent–voltage (J–V) characteristic curves of the cosensitized TiO_2/CdS/CdSe photoanode using various polymer gel electrolytes with and without the ZnSe passivation layer under solar radiation (AM 1.5 G) with a light intensity of 100 mW cm^{-2} are shown in Fig. 6a. The cosensitized TiO_2/CdS/CdSe photoanode using the prepared polymer gel electrolytes (SPU–GO) showed the high fill factor (FF) value of 0.55 and the open-circuit voltage (V_{oc}) is 0.51 V but the photocurrent density observed is low $J_{max} \sim 1.92$ mA cm^{-2}, resulting in a low power conversion efficiency (PCE) of $\eta = 0.51\%$, and hence, there is a need to improve the PCE. The power density–voltage curve is shown in Fig. 6b, which represents the variation of the maximum power output (P_{max}) under solar radiation. The open-circuit voltage (V_{oc}), short circuit current density (J_{sc}), FF and PCE (η) of these cells with various assemblies are presented in Table 3. The (SPU–GO–CC) polymer gel electrolytes and cosensitized TiO_2/CdS/CdSe photoanode with two SILAR cycles of ZnSe passivation layer showed the highest PCE ($\eta = 1.71\%$) with FF of 0.46 and open-circuit voltage (V_{oc}) of 0.73 V and short circuit current density (J_{sc}) of 5.09 mA cm^{-2} as compared to that without using any passivation layer. There are two optimisation parameters behind the high performance of the fabricated device. One is the high conductivity of the prepared polymer gel electrolytes by tagging graphene oxide in the pure polymer chain and subsequent addition of the optimized amount of conductive carbon (0.052%) in the prepared gel electrolytes due to which the charge transportation phenomena become fast. Another important step is the incorporation of ZnSe as the passivation layer on the cosensitized photoanode, which acts as a blocking layer of electrons and reduces the recombination of electron–hole pairs. The polymer gel electrolyte with 0.052 wt% conductive carbon (SPU–GO–CC) was prepared and used in QDSSCs, which exhibits low electrical resistance and high electrical conductivity causing enhanced photocurrent density by 1.92 to 2.89 mA cm^{-2} and open-circuit voltage from 0.51 to 0.55 V while the fill factor of QDSSCs decreases from 0.55 to 0.38. The power conversion efficiency of the cell increases from $\eta = 0.54$ to 0.60% of the QDSSCs due to the enhancement of the photocurrent density. The ZnSe passivation layer has been introduced between the cosensitized photoanode and polymer gel electrolytes, which plays an important role as an electron blocking layer (electron cannot pass onto gel electrolyte) while helping in charge transportation process of the hole transport from VB of CdSe to the HOMO level of the gel electrolyte through ZnSe layer because of the proximity of the energy level. Thereby, ZnSe acts as an effective passivation layer.

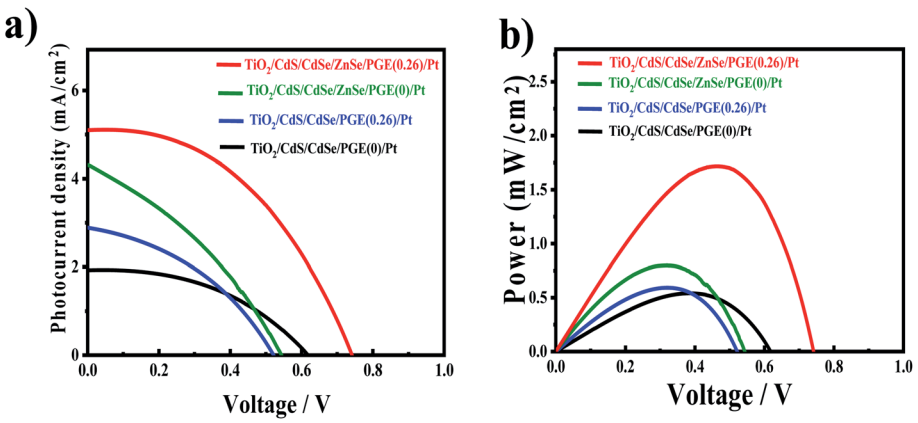

Fig. 6 (a) J–V characteristics measurement to calculate the photocurrent density and open-circuit voltage under 1 Sun illumination (100 mW cm^{-2}); and (b) power–voltage curve to calculate the power conversion efficiency (PCE) of the indicated QDSSCs.

Table 3 Open-circuit voltage (V_{oc}), short-circuit current density (J_{sc}), fill factor and power conversion efficiency, PCE (η) of various cells using the cosensitized photoanode and polymer gel electrolytes with and without the ZnSe passivation layer

Photoanode	J_{max} (mA cm^{-2})	V_{oc} (V)	Fill factor	Efficiency (%)
TiO_2/CdS/CdSe[a]	1.92	0.51	0.55	0.54
TiO_2/CdS/CdSe[b]	2.89	0.54	0.38	0.60
TiO_2/CdS/CdSe/ZnSe[a]	4.32	0.61	0.31	0.81
TiO_2/CdS/CdSe/ZnSe[b]	5.09	0.73	0.46	1.71

[a] Device using SPU–GO as the electrolyte. [b] Device using SPU–GO–CC composite gel electrolyte.

The performance of QDSSCs using the cosensitized TiO_2/CdS/CdSe photoanode and polymer gel electrolyte (SPU–GO) with the ZnSe passivation layer achieved PCE of $\eta = 0.81\%$ and photocurrent density J_{max} of 4.32 mA cm^{-2}, open-circuit voltage V_{oc} of 0.61 V, while the fill factor (FF) becomes 0.31. The high photocurrent density J_{max} of 5.09 mA cm^{-2}, open-circuit voltage (V_{oc}) of 0.73 V with a significant fill factor (FF) 0.46 with PCE of the QDSSCs, $\eta = 1.71\%$ was obtained by using the cosensitized TiO_2/CdS/CdSe photoanode and polymer gel electrolytes SPU–GO–CC with the ZnSe passivation layer. The better performance of the QDSSCs is due to the high electrical conductivity of polymer electrolytes obtained by adding the optimized amount of conductive carbon, which improves the better charge transportation and passivation layer and, thereby, play an important role, reducing the electron–hole recombination process and helping the charge (hole) transportation process between QDs and polymer gel electrolytes. This is to mention that negligible efficiency of $6.08 \times 10^{-9}\%$ was obtained using pure PU as the electrolyte gel from a poor J_{sc} of 5.2×10^{-6} mA cm^{-2}, while one order higher efficiency was achieved ($8.79 \times 10^{-8}\%$) by tagging the graphene moiety in PU (PU–GO as a gel electrolyte), which in turn indicates the superior effect of functionalization.

However, a novel polymer gel electrolyte is developed by tagging graphene oxide in the main chain followed by further chain extension and functionalization. The use of ZnSe as a passivation layer is helpful to restrict the recombination of electron–hole pairs by stopping the electron flow from ZnSe (conduction band) to gel electrolyte (LUMO level). The addition of a minute quantity of conducting carbon significantly improves the power conversion efficiency through the higher conductivity of the system. In gist, superior gel electrolyte along with modified stacking layers of cosensitizer and passivation layer revealed a much improved solar cell device.

Conclusions

Graphene oxide was chemically tagged in thermoplastic polyurethane chains of varying lengths through chain extenders such as butanediol. Polyurethane was further functionalized by attaching the sulfonate group to the main chain. The confirmation of chemical tagging of GO was understood through ^{1}H NMR, FTIR and UV spectroscopic measurements. The presence of graphene sheets reduced the electrical resistance (increasing conduction) of PU thermoplastics. Further, the ionic polar moiety enhanced the conductivity of GO-tagged PU (SPU–GO) and a semiconducting (1.07×10^{-3} S cm^{-1}) and a suitable gel electrolyte is developed for QDSSCs. The HOMO and LUMO energy levels of the functionalized polymers, depending upon the extent of fictionalizations, were measured through cyclic voltammetric measurements. Quantum dots, active materials like CdS and CdSe, were synthesized using suitable capping agents and their dimensions were measured through TEM bright-field images. The optical band gaps of the quantum dots were calculated using the light absorption measurements along with the relative light-harvesting efficiencies of individual and cosensitized systems. The electrical conductivity of functionalized polymer was increased by adding a minute quantity of conducting carbon (0.052%) and the HOMO/LUMO energy levels were optimized (close proximity) to the CB/VB of CdSe QDs. ZnSe has been used as a passivation layer, between the cosensitized photoanode and gel electrolytes, and the light-harvesting efficiency was increased by depositing ZnSe on active materials. Finally, the solar cell devices were fabricated by using the cosensitized photoanode with the ZnSe passivation layer and functionalized polyurethane coupled with the conducting carbon (SPU–GO–CC) gel electrolyte to obtain a power conversion efficiency of 1.71%. The roles of conducting carbon and passivation were explored as increasing the level of conduction and blocking the charge carriers as required to enhance the ultimate efficiency by reducing the chances of electrons–hole pair recombination.

Conflicts of interest

The authors declare no conflicts of interest.

Acknowledgements

RP is grateful to the institute (Indian Institute of Technology (BHU)) for providing the research fellowship. The use of instruments at the central facility is highly acknowledged.

References

1 D. Raja, B. Selvaraj, G. Shanmugam, A. Maruthapillai and D. Sundaramurthy, Improving the Efficiency of Dye-Sensitized Solar Cells via the Impact of Triphenylamine-Based Inventive Organic Additives on Biodegradable Cellulose Polymer Gel Electrolytes, *Energy Fuels*, 2021, **35**, 4273–4282.
2 A. Y. Hoekstra and T. O. Wiedmann, Humanity's unsustainable environmental footprint, *Science*, 2014, **344**, 1114–1117.
3 X.-B. Li, C.-H. Tung and L.-Z. Wu, Semiconducting quantum dots for artificial photosynthesis, *Nat. Rev. Chem.*, 2018, **2**, 160–173.
4 N. S. Lewis, Toward cost-effective solar energy use, *Science*, 2007, **315**, 798–801.

5 M. C. Hanna and A. J. Nozik, Solar conversion efficiency of photovoltaic and photoelectrolysis cells with carrier multiplication absorbers, *J. Appl. Phys.*, 2006, **100**, 74510.
6 K. Hara, *et al.*, Oligothiophene-containing coumarin dyes for efficient dye-sensitized solar cells, *J. Phys. Chem. B*, 2005, **109**, 15476–15482.
7 L. Yang, *et al.*, Highly efficient quantum dot-sensitized TiO_2 solar cells based on multilayered semiconductors (ZnSe/CdS/CdSe), *Nanoscale*, 2015, **7**, 3173–3180.
8 M. M. Lee, J. Teuscher, T. Miyasaka, T. N. Murakami and H. J. Snaith, Efficient hybrid solar cells based on meso-superstructured organometal halide perovskites, *Science*, 2012, **338**, 643–647.
9 G. E. Eperon, V. M. Burlakov, P. Docampo, A. Goriely and H. J. Snaith, Morphological control for high performance, solution-processed planar heterojunction perovskite solar cells, *Adv. Funct. Mater.*, 2014, **24**, 151–157.
10 S. Iijima, Helical microtubules of graphitic carbon, *Nature*, 1991, **354**, 56–58.
11 U. Bach, *et al.*, Solid-state dye-sensitized mesoporous TiO_2 solar cells with high photon-to-electron conversion efficiencies, *Nature*, 1998, **395**, 583–585.
12 P. Wang, *et al.*, A stable quasi-solid-state dye-sensitized solar cell with an amphiphilic ruthenium sensitizer and polymer gel electrolyte, *Nat. Mater.*, 2003, **2**, 402–407.
13 W. W. Yu, L. Qu, W. Guo and X. Peng, Experimental determination of the extinction coefficient of CdTe, CdSe, and CdS nanocrystals, *Chem. Mater.*, 2003, **15**, 2854.
14 H. Tada, M. Fujishima and H. Kobayashi, Photodeposition of metal sulfide quantum dots on titanium(IV) dioxide and the applications to solar energy conversion, *Chem. Soc. Rev.*, 2011, **40**, 4232–4243.
15 A. Subramanian, *et al.*, Improved photovoltaic performance of quantum dot-sensitized solar cells using multi-layered semiconductors with the effect of a ZnSe passivation layer, *New J. Chem.*, 2017, **41**, 5942–5949.
16 S. Lu, *et al.*, Impacts of Mn ion in ZnSe passivation on electronic band structure for high efficiency CdS/CdSe quantum dot solar cells, *Dalton Trans.*, 2018, **47**, 9634–9642.
17 N. Firoozi, H. Dehghani and M. Afrooz, Cobalt-doped cadmium sulfide nanoparticles as efficient strategy to enhance performance of quantum dot sensitized solar cells, *J. Power Sources*, 2015, **278**, 98–103.
18 R. Zhou, *et al.*, A novel anion-exchange strategy for constructing high performance PbS quantum dot-sensitized solar cells, *Nano Energy*, 2016, **30**, 559–569.
19 W. Shockley and H. J. Queisser, Detailed Balance Limit of Efficiency of p–n Junction Solar Cells, *J. Appl. Phys.*, 1961, **32**, 510–519.
20 O. E. Semonin, *et al.*, Peak External Photocurrent Quantum Efficiency Exceeding 100% via MEG in a Quantum Dot Solar Cell, *Science*, 2011, **334**, 1530–1533.
21 J. Huang, *et al.*, Improved Performance of Colloidal CdSe Quantum Dot-Sensitized Solar Cells by Hybrid Passivation, *ACS Appl. Mater. Interfaces*, 2014, **6**, 18808–18815.
22 J. B. Sambur and B. A. Parkinson, CdSe/ZnS Core/Shell Quantum Dot Sensitization of Low Index TiO_2 Single Crystal Surfaces, *J. Am. Chem. Soc.*, 2010, **132**, 2130–2131.
23 Q. Shen, J. Kobayashi, L. J. Diguna and T. Toyoda, Effect of ZnS coating on the photovoltaic properties of CdSe quantum dot-sensitized solar cells, *J. Appl. Phys.*, 2008, **103**, 84304.
24 S. Verma, S. Kaniyankandy and H. N. Ghosh, Charge Separation by Indirect Bandgap Transitions in CdS/ZnSe Type-II Core/Shell Quantum Dots, *J. Phys. Chem. C*, 2013, **117**, 10901–10908.
25 F. Huang, *et al.*, Doubling the power conversion efficiency in CdS/CdSe quantum dot sensitized solar cells with a ZnSe passivation layer, *Nano Energy*, 2016, **26**, 114–122.
26 F. Huang, *et al.*, Impacts of surface or interface chemistry of ZnSe passivation layer on the performance of CdS/CdSe quantum dot sensitized solar cells, *Nano Energy*, 2017, **32**, 433–440.
27 V. Jovanovski, *et al.*, A Sulfide/Polysulfide-Based Ionic Liquid Electrolyte for Quantum Dot-Sensitized Solar Cells, *J. Am. Chem. Soc.*, 2011, **133**, 20156–20159.
28 P. K. Santra and P. V. Kamat, Mn-doped quantum dot sensitized solar cells: a strategy to boost efficiency over 5%, *J. Am. Chem. Soc.*, 2012, **134**, 2508–2511.
29 M. S. Su'ait, M. Y. A. Rahman and A. Ahmad, Review on polymer electrolyte in dye-sensitized solar cells (DSSCs), *Sol. Energy*, 2015, **115**, 452–470.
30 D. E. Fenton, Complexes of alkali metal ions with poly(ethylene oxide), *Polymer*, 1973, **14**, 589.
31 F. Bella and R. Bongiovanni, Photoinduced polymerization: an innovative, powerful and environmentally friendly technique for the preparation of polymer electrolytes for dye-sensitized solar cells, *J. Photochem. Photobiol., C*, 2013, **16**, 1–21.
32 R. Prakash and P. Maiti, Functionalized Thermoplastic Polyurethane Gel Electrolytes for Cosensitized TiO_2/CdS/CdSe Photoanode Solar Cells with High Efficiency, *Energy Fuels*, 2020, **34**, 16847–16857.
33 S. Kumar, Functionalized Thermoplastic Polyurethane as Hole Conductor for Quantum Dot-Sensitized Solar Cell, *ACS Appl. Energy Mater.*, 2018, **1**, 4641.
34 N. Yousefi, *et al.*, Highly aligned, ultralarge-size reduced graphene oxide/polyurethane nanocomposites: mechanical properties and moisture permeability, *Composites, Part A*, 2013, **49**, 42–50.
35 R. Shamsi, M. Koosha and M. Mahyari, Improving the mechanical, thermal and electrical properties of polyurethane–graphene oxide nanocomposites synthesized by in-situ polymerization of ester-based polyol with hexamethylene diisocyanate, *J. Polym. Res.*, 2016, **23**, 1–11.
36 D. Saxena, D. Rana, E. Bhoje Gowd and P. Maiti, Improvement in mechanical and structural properties of poly(ethylene terephthalate) nanohybrid, *SN Appl. Sci.*, 2019, **1**, 1363.
37 A. Gaur, D. Rana and P. Maiti, Mechanical and wear behaviour of poly(vinylidene fluoride)/clay nanocomposite, *J. Mater. Res. Technol.*, 2019, **8**, 5874.

38 K. K. Jana, Functionalized poly(vinylidene fluoride) nanohybrid for superior fuel cell membrane, *J. Membr. Sci.*, 2015, **481**, 124.
39 D. Saxena, N. Soundararajan, V. Katiyar, D. Rana and P. Maiti, Structural, mechanical, and gas barrier properties of poly(ethylene terephthalate) nanohybrid using nanotalc, *J. Appl. Polym. Sci.*, 2020, **137**, 48607.
40 W. William and X. Peng, Formation of High-Quality CdS and Other II–VI Semiconductor Nanocrystals in Noncoordinating Solvents: Tunable Reactivity of Monomers, *Angew. Chem., Int. Ed.*, 2002, **41**, 2368.
41 Z. A. Peng and X. Peng, Formation of high-quality CdTe, CdSe, and CdS nanocrystals using CdO as precursor, *J. Am. Chem. Soc.*, 2001, **123**, 183.
42 D. C. Marcano, D. V. Kosynkin, J. M. Berlin, A. Sinitskii, Z. Sun, A. Slesarev, L. B. Alemany, W. Lu and J. M. Tour, Improv. Synth. Graphene Oxide, *ACS Nano*, 2010, **4**, 4806.
43 D. K. Patel, Functionalized Graphene Tagged Polyurethanes for Corrosion Inhibitor and Sustained Drug Delivery, *ACS Biomater. Sci. Eng.*, 2017, **3**, 3351.
44 L. Leonat, G. Sbarcea and I. V. Branzoi, *UPB Scientific Bulletin, Series B: Chemistry and Materials Science*, 2013, **75**, 111.
45 M. Suen, H. Lee, H. Chen and C. Chen, Water remaining properties of nonwoven fabrics treated with the polyurethane polymers containing carboxylic acid group and the thermal and structural characterization of the polymers, *J. Appl. Polym. Sci.*, 2008, **107**, 2618–2625.
46 D. K. Patel, *et al.*, Graphene as a chain extender of polyurethanes for biomedical applications, *RSC Adv.*, 2016, **6**, 58628–58640.
47 S. Banerjee, Highly efficient polyurethane ionomer corrosion inhibitor: the effect of chain structure, *RSC Adv.*, 2011, **1**, 199.
48 B.-O. Jung, J. Na and C. H. Kim, Synthesis of chitosan derivatives with anionic groups and its biocompatibility in vitro, *J. Ind. Eng. Chem.*, 2007, **13**, 772.
49 C. E. Fernández, Crystal structure and morphology of linear aliphatic *n*-polyurethanes, *Macromolecules*, 2010, **43**, 4161.
50 C. S. Wong and K. H. Badri, Chemical analyses of palm kernel oil-based polyurethane prepolymer, *Mater. Sci. Appl.*, 2012, 78–86.
51 Y. Chen, S. Zhou, H. Yang and L. Wu, Structure and properties of polyurethane/nanosilica composites, *J. Appl. Polym. Sci.*, 2005, **95**, 1032–1039.
52 S.-W. Wang and R. H. Colby, Linear Viscoelasticity and Cation Conduction in Polyurethane Sulfonate Ionomers with Ions in the Soft Segment–Single Phase Systems, *Macromolecules*, 2018, **51**, 2757–2766.
53 T. Radhakrishnan, M. K. Georges, P. Sreekumari Nair, A. S. Luyt and V. Djoković, Composites comprising CdS nanoparticles and poly(ethylene oxide): optical properties and influence of the nanofiller content on the thermal behaviour of the host matrix, *Colloid Polym. Sci.*, 2008, **286**, 683–689.
54 D. K. Dwivedi, D. Shankar and M. Dubey, Synthesis, structural and optical characterization of CdS nanoparticles, *J. Ovonic Res.*, 2010, **6**, 57–62.
55 R. K. Duchaniya, Optical studies of chemically synthesis CdS nanoparticles, *Int. J. Mining, Metall. Mech. Eng.*, 2014, **2**, 54–56.
56 P. Tao, Y. Li, R. W. Siegel and L. S. Schadler, Transparent luminescent silicone nanocomposites filled with bimodal PDMS-brush-grafted CdSe quantum dots, *J. Mater. Chem. C*, 2013, **1**, 86.
57 B. Fritzinger, R. K. Capek, K. Lambert, J. C. Martins and Z. Hens, Utilizing self-exchange to address the binding of carboxylic acid ligands to CdSe quantum dots, *J. Am. Chem. Soc.*, 2010, **132**, 10195.
58 F. Huang, *et al.*, Impacts of surface or interface chemistry of ZnSe passivation layer on the performance of CdS/CdSe quantum dot sensitized solar cells, *Nano Energy*, 2017, **32**, 433–440.